EM11/Dan Hipp

Final Report

for

UAH Contract NAS8-38609 D. O. 50

Mass Analysis Addition to the Differential Ion Flux Probe (DIFP) Study

Dr. K. H. Wright, Jr. and Richard Jolley
Center for Space Plasma and Aeronomic Research
The University of Alabama Huntsville
Huntsville, AL 35899

(NASA-CR-196531) MASS ANALYSIS ADDITION TO THE DIFFERENTIAL ION FLUX PROBE (DIFP) STUDY Final Report (Alabama Univ.) 34 p

N95-15824

Unclas

G3/19 0030497

ABSTRACT

The objective of this study is to develop a technique to measure the characteristics of space plasmas under highly disturbed conditions; e.g., non-Maxwellian plasmas with strong drifting populations and plasmas contaminated by spacecraft outgassing. The approach to meet this objective, conducted in conjunction with current MSFC/ES83 activities, is to extend the capabilities of the Differential Ion Flux Probe (DIFP) to include a high throughput mass measurement that does not require either high voltage or contamination sensitive devices such as channeltron electron multipliers or microchannel plates. This will significantly reduce the complexity and expense of instrument fabrication, testing, and integration of flight hardware compared to classical mass analyzers. The feasibility of the enhanced DIFP has been verified by using breadboard test models in a controlled plasma environment. The ability to manipulate particles through the instrument regardless of incident angle, energy, or ionic component has been amply demonstrated. The energy analysis mode is differential and leads directly to a time-of-flight mass measurement. With the new design, the DIFP will deconvolve multiple ion streams and analyze each stream independently for ion flux intensity, velocity (including direction of motion), mass, and temperature (or energy distribution). In particular, such an instrument will be invaluable on follow-on electrodynamic TSS missions and, possibly, for environmental monitoring on the space station Freedom.

1.0 INTRODUCTION

With our improved comprehension of the complexity of plasma processes involved in the earth's magnetosphere and in the local, perturbed environment of a spacecraft, the need for more sophisticated measurements and a more careful assessment of spacecraft environmental effects has become apparent. For example, it appears that spacecraft charging effects were erroneously interpreted as either a wake traversal of the satellite Ganymede or a "bubbling" state of the Jovian magnetospheric plasma [*Khurana et al.*, 1987]. The effect of spacecraft-space plasma interactions was further emphasized by the results of the STS-3 and Spacelab-2 missions, where outgassed contaminents produced a co-orbiting neutral gas cloud that surrounded the space shuttle and significantly modified the physics of its interaction with the ionosphere [*Pickett et al.*, 1985; *Paterson and Frank*, 1989]. In addition, with the renewal of space shuttle missions, active experiments involving perturbing influences, such as charged particle beam injections, high power rf wave injections, and plasma modification via gas injections are planned. Clearly, we must deal with highly perturbed situations that represent strong departures from the ambient conditions for which the majority of the existing plasma instrumentation was designed.

This investigation supported MSFC/ES83 activities to develop plasma instrumentation that could be available for sub-orbital and orbital missions in order to, not only investigate spacecraft-space plasma interactions, but also to investigate the acceleration of charged particles in the polar regions of the magnetosphere. Such accelerations are an important aspect of natural phenomena such as the polar wind and other high latitude plasma outflows by which particles escape the ionosphere and populate the terrestrial magnetosphere [*Chappell et al.*, 1987]. Spacecraft that are positioned to study these processes will pass through highly disturbed, non-equilibrium plasmas and require the type instrumentation examined herein. For example, this instrument will provide measurements of the early development of ion conics in the ionospheric plasma and is able to deconvolve

these effects from the effects of spacecraft charging [*Stone et al.*, 1988*a*; *Katz and Davis*, 1988].

2.0 OBJECTIVE

The standard Differential Ion Flux Probe (DIFP) [e. g., *Stone*, 1977] is capable of deconvolving multiple ion streams incident at a single point in space. Measurements of the ion flow direction, drift energy, current density, and temperature for each individual ion stream are performed. However, vector ion flux measurements cannot be fully analyzed without a knowledge of the ion mass of each individual stream. When multiple streams exist, it is neccessary to deconvolve them unambiguously and assign a mass to each stream. In the data obtained from existing instruments, an uncertainty exists in the mass assignment in the event of multiple streams and multiple ions; i.e., it is presently necessary to assume either the ion mass or the drift velocity – neither being strictly valid in the polar region where hydrogen, helium, and oxygen may each contribute to the plasma behavior, or in the plasma environment of a spacecraft where pick-up of ionized contaminents negates the assumption of both typical ionospheric composition and orbital velocity. (Note that a classical ion mass spectrometer does not remove this ambiguity.)

Therefore, the objective of UAH's effort, together with that of MSFC/ES83, is to develop a technique for measuring the ion mass associated with each individual ion stream in nonparallel plasma flows that can become an integral part of the existing DIFP instrument. We will continue to pursue techniques that do not require high voltage or contamination sensitive devices such as channeltron electron multipliers or microchannel plates because of the additional complexity of the instrument design and interface requirements.

3.0 APPROACH

3.1 Brief Instrument History

The DIFP instrument was developed in-house at MSFC to meet unique measurement requirements in laboratory plasma investigations [*Stone*, 1977]. These studies examined

the complex particle behavior in the wake region of bodies placed in collisionless, supersonic, single-ion plasma flows. Among the particle disturbances diagnosed by the DIFP was the converging of spatially limited, multiple ion streams onto the wake axis [*Stone*, 1981]. Further wake studies were performed in two-ion plasma flows where the DIFP was also used to obtain the key measurements [*Wright*, 1987]. Since each ion mass was known in these experiments, thereby removing the mass/drift velocity ambiguity, the motion of each ion species could be determined.

Based on the laboratory research performed at MSFC, the DIFP was subsequently redesigned for space flight [*Stone et al.*, 1985]. During the OSS-1/STS-3 mission, the DIFP provided the first differential vector measurements of the complex ion flow field in the local environment of an orbiting vehicle [*Stone et al.*, 1983, 1986]. The same instrument was reflown on the Spacelab-2 mission and performed measurements in the wake of the shuttle – an object much larger than any previous orbiting satellite. Results from this mission showed that the particle behavior in the near wake of the shuttle is remarkably similar to that observed in ground-based laboratory experiments which use small bodies [*Stone et al.*, 1988*b*].

The basic DIFP sensor design is currently part of the MSFC-developed Research on Orbital Plasma Electrodynamics (ROPE) experiment that flew on the first mission of the Tethered Satellite System (TSS-1) during August 1992. The electronics to control the operation of the ROPE/DIFP were upgraded from the previous flight model. An eight bit microprocessor was incorporated to provide additional capabilities and more flexibility in the control logic. This modification will allow the instrument to be reconfigured for different applications more easily and will permit the addition of new capabilities, such as the proposed mass analysis.

Previous efforts to develop a mass measurement technique to combine with the DIFP sensor included using the well known Bennett RF technique [*Bennett*, 1950]. The advantage of the RF technique is its simplicity, its relatively large entrance aperature, and its

ability to collect measureable current without using electron multipliers and high voltage. A number of variations of the Bennett technique were breadboarded and extensively tested at MSFC. However, these techniques did not meet the design criteria of a sufficiently high current throughput and sharp mass analysis over the range of 0 to 50 AMU [*Carruth*, 1989].

3.2 Proposed Test Design

To enhance the DIFP to accomodate an ion mass analysis, the initial test design is to use the DIFP ion deflection and collimation electro-optics to gate the ions for a time-of-flight measurement. This approach is potentially superior to the Bennett technique in that it will require no grids. The Bennett technique requires approximately 10 grids, which greatly reduces overall sensitivity.

A conceptual sketch of the new technique is shown in Figure 1. The first deflection plate followed by a collimator is taken from the existing DIFP sensor design. This section is used to determine the angle of incidence of positive ions. Three additional deflection plates (or "gates") have been added to the original DIFP design below the collimator. The magnitude of the required bias voltage in the three-gate section gives a direct measurement of the ion energy (trajectory B) while the ion mass is determined by modulating the bias voltages to gate the ion stream to allow time-of-flight measurements (trajectory A). Note that by forcing particles to follow a curved path in the lower section allows a differential measurement of energy. This is a different technique than the gridded planar retarding potential method used in the original DIFP.

Hereafter, a shorthand notation for the instrument under study will be used: DIFPM – which means DIFP with Mass analysis.

3.3 Test Sequence

The test flow for the DIFPM study was as follows: (1) computer ray tracing was used to investigate design feasibility and spacing between deflection plates. The program was operated by MSFC/ES83 personnel. (2) Promising designs were breadboarded and tested

in the MSFC Space Science Laboratory space plasma research facilities under ionospheric conditions (i.e., under similar values of ion drift velocity, plasma temperature, and plasma density). A rotatable turntable allowed investigation of the required angular response range. The accelerating voltage supply currently used in the plasma source covers beam energies up to 80 eV. Working gases of N_2^+ (28 AMU), Ar^+ (40 AMU), and Kr^+ (84 AMU) were used. Data was recorded with standard X-Y plotters. A computer data acquisition system was available and was prepared for use with the DIFPM, but was not used for reasons discussed later in the text. A laboratory model of the flight DIFP sensor design that is convertable to a standard, planar RPA was used to monitor the plasma stream during testing. (3) Test data were carefully analyzed to determine the viability of the proposed DIFPM design.

4.0 RESULTS FOR THE THREE-GATE DESIGN

Figure 2 shows an example of computer ray tracing of the "three-gate" design – DIFPM design no. 1.1. Particles enter the instrument at the top of the diagram. Bias voltages (ϕ_1, ϕ_2, ϕ_3) are applied to the diagonal surfaces, with the polarity indicated by the +, – signs. The stacked array of deflection plates focusses particles through the instrument. The trajectory shown in Figure 2 corresponds to the mass analysis trajectory indicated by "A" in Figure 1. A breadboard instrument was built to the dimensions indicated on Figure 2. Each deflection plate and collimator consisted of 10 slits.

The deflection plate labeled ϕ_1 serves as the angular discriminator. The angular range of measurement does extend to $\pm 45°$ while the angular sensitivity of the DIFPM is slightly less than that for the standard DIFP. The reduced data for the angular behavior will be presented later in section 5.0. The throughput for design 1.1 is 0.41 as compared with 0.23 for the standard DIFP. It is noted that the voltages needed for instrument operation in the lab are less than that predicted by the computer ray tracing. This indicates that the electric field in the model is less than the actual case. The utility of the computer ray tracing therefore lies not in its quantitative prediction but in serving as a guide for test

designs. Calibration equations describing the DIFPM must therefore be totally determined from laboratory data.

Figure 3 presents data concerning the energy analysis operation. Ion trajectories are shown Figure 3*a* while the detector response for each trajectory is displayed in Figure 3*b*. A voltage sweep is applied to ϕ_2 and the opposite polarity applied to ϕ_3 while ϕ_1 and ϕ_4 remain constant. If the voltage value at the peak of the response curve (labeled with $*$) is plotted versus beam energy, then the energy calibration curve is obtained. That relationship is shown in Figure 3*c* and appears to be linear.

The operation of the DIFPM for the mass analysis mode is depicted in Figure 4. Note that the voltages required for the trajectories shown in Figure 4*a* are larger than those needed for the energy measurement. The detector response for these trajectories is indicated in Figure 4*b*. A voltage sweep is applied to ϕ_3 while ϕ_1, ϕ_2, and ϕ_4 remain constant. The asymmetries and extraneous peaks seen in the output are due to misalignment of the deflection plates and/or collimators and cross-talk between channels. Improved alignment between the internal components, increased height of the collimators, and a change in spacing between the deflection plates are expected to clean-up the output signal.

The ability to control particles through the instrument in a desired manner has been demonstrated. However, problems were encountered when test voltages were modulated at RF frequencies in order to examine the mass analysis capability. The electrometer located inside the instrument had a severe noise pick-up problem that would mask any "real" output signal. A change in signal grounding on the electrometer board corrected this problem and was incorporated in a new instrument design described in the following section.

MSFC/EB24 personnel developed an RF voltage source for use with our plasma chamber testing. This circuit also serves as the initial development of part of the flight electronics for the DIFPM. The magnitude of voltage required of this circuit as dictated by the operation shown in Figure 3*a* was beyond initial design capabilities. To simplify instrument

operation and also accomodate the RF circuit capability, a "four-gate" design was constructed. With the new design, less voltage was expected to be required to focus particles through the instrument.

5.0 RESULTS FOR THE FOUR-GATE DESIGN

The four-gate instrument configuration is referred to as design no. 2.1. Particle ray-tracing through this design is shown in Figure 5. Approximately the same spacing between deflection plates was used in this model as in design no. 1.1. The mass analysis trajectory is again simulated. Note that (1) all of the deflection plates in the mass/energy anaylsis section are operated at the same voltage thereby simplifying operation and (2) the curvature of the particles is less than that shown in Figure 2*a* which could enhance throughput.

The configuration of the actual test hardware was different from the computer model. In a continueing effort to reduce the required applied voltages, the spacing between the plates in the energy/mass analysis section was doubled to 0.75 inches as compared with the computer model and design no. 1.1. In addition, the top and bottom collimators were made to be the same height.

5.1 Angular response and throughput

The angular response of design no. 2.1 is demonstrated in Figure 6 with the raw data. A voltage sweep is applied to ϕ_1 while ϕ_2, ϕ_3, ϕ_4, and ϕ_5 remain constant at zero volts. Plasma conditions for this data are ion mass = N_2^+ and beam energy = 37 eV. Note the smooth variation in the envelope of the amplitudes with increasing angle-of-attack. For angles 30° – 45°, the DIFPM output has been multiplied by two.

The reduced angular response data for several energies and all masses is presented in Figure 7. For comparison, the curves describing the Spacelab 2/DIFP performance are included. In Figure 7*a*, the angle calibration curve is obtained by plotting (plate voltage at the response curve peak/particle energy) versus angle-of-attack. For a given angle and energy, DIFPM design no. 2.1 requires a slightly higher plate voltage than the Spacelab 2/DIFP version. To keep instrument voltages down and maintain the same angular sample

range, the DIFPM front end should be modified by slightly increasing the drift region between plate 1 and the top collimator. Further ray tracing can guide how much the increase should be.

In Figure 7*b*, the angular sensitivity is displayed. The present instrument is shown to be more sensitive with angle as compared to the Spacelab 2/DIFP. Note that the data points are quite scattered. This resulted from an observed capacitance involving the plates and possibly differences in the magnitudes of the lab generated voltages applied across the slits. Recall that the applied voltage should be of equal magnitude but opposite polarity. The response curve shifted both in voltage location and in amplitude according to the direction of the ϕ_1 sweep. The convention used to acquire all data for the X-Y plotter in this study was to begin a voltage sweep at zero and move in the appropriate positive or negative direction as required. This capacitance (or charging) effect could influence the exact quantitative values for the instrument operation in any mode. However, the gross behavior of the instrument responses is very repeatable and correction of the above problem for flight application should have only second order effects in the quantitative calibration curves presented in this report.

The throughput for particles entering the instrument approximately along the normal is 0.3. This value is lower than that for design no. 1.1 (0.41), not surprising since an extra plate exists, but the throughput appears to be slightly higher than the standard DIFP. The goal of a relatively high throughput for the DIFPM is achieved.

5.2 Energy analysis mode

The energy analysis operation results are displayed in Figure 8. The particle trajectories are indicated in Figure 8*a* while the instrument response for each trajectory is noted in Figure 8*b*. The instrument response is obtained by applying a voltage sweep to ϕ_2 and ϕ_3 (with opposite polarity) and maintaining ϕ_4 and ϕ_5 at zero volts. The incident plasma stream is approximately aligned with the instrument normal. ϕ_1 is chosen to maximize the throughput. Note that extra peaks appear, denoted by the dots, as compared with the

profile shown in Figure 3*b*. Those peaks were also present in the energy analysis operation of design no. 1.1 but not shown so as to emphasize proof of concept. The energy calibration curve for the main peak (denoted by $*$), obtained over the energy range 20 – 70 eV using all three masses, is presented in Figure 8*c*. The values for the positive and negative peaks were averaged for the plot. The data are described by the following linear equation

$$\phi_E = a_1 E + b_1, \tag{1}$$

where ϕ_E = voltage at the peak, E = the beam energy, $a_1 = 0.323$ (Volts/eV), and $b_1 = 0.07$ Volts. Note that the linear correlation coefficient $r = 0.995671$ is quite close to 1.

The extra or "ghost" peaks also have a linear function with beam energy. The amplitude ratio of the secondary to main peak also has a preferred value. This information can be used to discriminate between main and secondary peaks during energy analysis for a plasma input with unknown properties.

The variation of the instrument response in the energy analysis mode for non-zero angles-of-attack is illustrated in Figure 9. The voltage location of the peaks changes slightly. The shift in peak voltage can increase with increasing angle. However, it is believed that the correction with angle to the energy calibration curve is a second order effect.

5.3 Mass analysis mode

The results for phase 1 of the mass analysis mode are displayed in Figure 10. Phase 1 consists of selecting the appropriate particle trajectory (see Figure 10*a*). The instrument response for each trajectory is noted in Figure 10*b*. The instrument response is obtained by applying a voltage sweep to ϕ_2, ϕ_3, ϕ_4, and ϕ_5 in unison with the indicated polarity in Figure 10*a*. Again the incident plasma stream is approximately aligned with the instrument normal and ϕ_1 is chosen to maximize the throughput. Note the similarity in response with that of the energy analysis mode shown in Figure 8*b*. Also note how the response is much

cleaner relative to design no. 1.1 (see Figure 4*b*). The relationship of the voltage location of the main peak (denoted by $*$) to the beam energy is presented in Figure 10*c* and described by the following linear equation:

$$\phi_M = a_2 E + b_2, \tag{2}$$

where ϕ_M = voltage at the peak, E = the beam energy, $a_2 = 0.377$ (Volts/eV), and $b_1 = -0.6$ Volts. Note that the linear correlation coefficient $r = 0.99056$ is quite close to 1. For ideal instrument operation, a_1 from Eq. (1) should be the same as a_2 from Eq. (2). For the data shown the difference is about 17% . This small difference means that if the voltage for the main peak in the energy analysis mode is used to define the mass analysis trajectory, very little particle flux is lost.

The variation of the instrument response in phase 1 of the mass analysis mode for non-zero angles-of-attack is illustrated in Figure 11. The simplest presentation is to compare the energy analysis trajectory with the mass analysis trajectory at the same angle. The voltage location of the peaks changes slightly. The shift in peak voltage can increase with increasing angle. This means that progressively more flux is lost in changing from the energy analysis mode to the mass analysis mode at the higher angles-of-attack. Note that an additional small amplitude peak appears in the mass trajectory mode. This ghost peak is always present in the non-zero angles-of-attack. Changes in the bottom collimator height and/or location is expected to eliminate this ghost peak.

Phase 2 of the mass analysis mode is the time-of-flight technique. Modulating the peak voltage applied to the plates determined from the energy analysis mode (ϕ_E) introduces timed 'gates' that particles with only a certain velocity V (or mass M) can pass through, since $V \propto (E/M)^{\frac{1}{2}}$. The frequency of the gate operation is given simply by

$$f = V/d, \tag{3}$$

where d = the distance between gates. The modulating wave form should be a square wave with amplitude $+\phi_E$ to $-\phi_E$. In this manner, both of the dashed-lined trajectories

of Figure 10*a* contribute to the instrument response. For the plate spacing of design no. 2.1, the range of plasma energies needed, and the available working gases, the RF circuit used in this test phase was required to provide a square wave up to 1 MHz at $+40$ to -40 Volts amplitude.

Figure 12 shows the instrument response as a function of frequency. As noted above the value for the frequency at which the particle flux should peak is $f \propto V \propto (E/M)^{\frac{1}{2}}$. In Figure 12*a*, the output for various ion masses at the same beam energy is displayed. An arrow indicates the main peak for a given ion mass. Note that as ion mass increases, the peak frequency decreases, as expected. Several ghost peaks of much smaller amplitude than the main peak occur. Changes in the spacing between plates and a change in the bottom collimator characteristics could probably eliminate these ghosts. For the Kr^+ case, the main peak occurs at approximately 475 kHz. We also expect to see a peak at integral multiples of the main peak frequency and indeed that is the case as a secondary peak of lower intensity is observed at about 950 kHz. The main peak in each case is clearly the dominant signal. In Figure 12*b*, instrument output for various energies at a constant mass is displayed. An arrow locates the main peak for each energy. As the energy increases, the peak frequency increases, as expected. Ghosts peaks are observed again as well as the 2f peak for the 20.5 eV case.

The reduced data for the mass (time-of-flight) calibration curve is shown in Figure 13. The frequency of the main peak is plotted as a function of ion velocity. The data are described by the following equation:

$$F = a_3 V + b_3, \tag{4}$$

where F = frequency of the main peak, $V = (2qE/M)^{\frac{1}{2}}$, q = electronic charge, $a_3 = 45.02(\frac{kHz}{km/s})$, and b = -9.9 kHz. The linear correlation coefficient is r = 0.99813. In comparing Eq. (4) with Eq. (3), we find that $1/a_3 = 2.221$ cm should represent the effective distance between succesive time-of-flight gates. The distance between the slit aperature of successive plates for design no. 2.1 is 0.75" (spacing) + 0.0625" (plate thickness) = 2.064

cm. The small difference between the estimated and the measured distances verifies the time-of-flight technique.

The variation of the instrument response with angle-of-attack is shown in Figure 14. The ion mass and drift energy of the plasma were held constant. The ϕ_1 and ϕ_E voltages were chosen to maximize throughput before the modulation was applied. The frequency position of the main peak is basically the same with at most a second order correction for angle.

6.0 SUMMARY

The standard DIFP has been upgraded to include mass analysis. The feasibility of the new design has been verified through testing in a drifting plasma environment. The angular response over $-45°$ to $+45°$ remains qualitatively the same as before. A minor change in the front end should enable the reproduction of the previous flight model calibration results. In the new configuration, the section below the angle selection front end has been replaced by a stack of four deflection plates – the "four-gate" design. Each deflection plate is identical to the standard deflection plate used in the past. The ability to manipulate particles through the four-gate design in both the energy and mass analysis modes has been demonstrated. The instrument response for energy analysis operation is differential in nature and linear with respect to applied plate voltage. The four-gate design allows simple operation in the mass analysis mode in that all four deflection plates use the same magnitude of applied voltage. Modulation of the plate voltage produces a true time-of-flight measurement such that the frequency at the peak response is a linear function of particle velocity. Instrument throughput is about 25% higher than the previous DIFP. The results of this study serve as the foundation to construct a flight model that can be used to diagnose multi-component, drifting, non-Maxwellian plasmas.

Acknowledgement. We would like to thank various people at MSFC for their help in the completion of this study: Dr. Nobie Stone (ES83) for developing the instrument concept and for discusions during the course of this study; Bill Chisholm, Bill Bond, Chuck Ryland

(all at ES93) for the fabrication and assembly of the test hardware; Dennis Smith (EB25) for the various electronic circuits; and Victoria Coffey (ES83) for assistance in the computer ray tracing. The effort expended by MSFC and UAH during this task will clear an initial developmental hurdle so that more advanced instrumentation can be proposed for future flights. This will have the effect of enhancing (1) the chance for selection of future proposals for flight investigations using MSFC and UAH personnel, and (2) the quality of the experiment and its scientific return.

REFERENCES

Bennett, W. H., Radiofrequency mas spectrometer, *J. Applied Physics*, *21*, 143, 1950.

Carruth, Jr., M. R., Re-examination of radiofrequency mass spectrometers, Center Director's Discretionary Fund Final Report, NASA Technical Memorandum 100353, January, 1989.

Chappell, C. R., T. E. Moore, J. H. Waite, Jr., The ionosphere as a fully adequate source of plasma for the earth's magnetosphere, *J. Geophys. Res.*, *92*, 5896, 1987.

Katz, I. and V. A. Davis, Reply, *J. Geophys. Res.*, *93*, 4149, 1988.

Khurana, K. K., M. G. Kivelson, T. P. Armstrong, and R. J. Walker, Voids in Jovian Magnetosphere revisited: Evidence of spacecraft charging, *J. Geophys. Res.*, *92*, 13399, 1987.

Paterson, W. R.and L. A. Frank, Hot ion plasmas from the cloud of neutral gases surrounding the Space Shuttle, *J. Geophys. Res.*, *94*, 3721, 1989.

Pickett, J. S., G. B. Murphy, W. S. Kurth, C. K. Goertz, and S. D. Shawhan, Effects of chemical releases by the STS-3 Orbiter on the ionosphere, *J. Geophys. Res.*, *90*, 3487, 1985.

Stone, N. H., Technique for measuring the differential ion flux vector, *Rev. Sci. Instru.*, *48*, 1458, 1977.

Stone, N. H., The plasma wake of mesosonic conducting bodies. Part 1. An experimental parametric study of ion focussing by the plasma sheath, *J. Plasma Physics*, *25*, 351, 1981.

Stone, N. H., U. Samir, K. H. Wright, Jr., D. L. Reasoner, and S. D. Shawhan, Multiple ion streams in the near vicinity of the space shuttle, *Geophys. Res. Lett.*, *10*, 1215, 1983.

Stone, N. H., B. J. Lewter, W. L. Chisholm, and K. H. Wright, Jr., An instrument for differential ion flux measurements on Spacelab-2, *Rev. Sci. Instru.*, *56*, 1897, 1985.

Stone, N. H., K. H. Wright, Jr., K. S. Hwang, U. Samir, G. B. Murphy, and S. D. Shawhan, Further observations of Space Shuttle plasma-electrodynamic effects from OSS-1/STS-3, *Geophys. Res. Lett.*, *13*, 217, 1986.

Stone, N. H., U. Samir, K. H. Wright, Jr., and K. S. Hwang, Comment on "Ram ion scattering by Space Shuttle V x B induced differential charging" by I. Katz and V. A. Davis, *J. Geophys. Res.*, *93*, 4143, 1988*a*.

Stone, N. H., K. H. Wright, Jr., U. Samir, and K. S. Hwang, On the expansion of ionospheric plasma into the near-wake of the space shuttle Orbiter, *Geophys. Res. Lett.*, *15*, 1169, 1988*b*.

Wright, Jr., K. H., A study of single and binary ion plasma expansion into laboratory-generated plasma wakes, PhD thesis, The University of Alabama in Huntsville, December 1987, and *NASA CR-4125*, February 1988.

FIGURE CAPTIONS

Figure 1. Schematic of a conceptual design for an integrated DIFP/mass measurement technique that makes use of the DIFP electro-optics. Ion trajectory A represents the "gated" mass measurement mode, while trajectory B represents the angle and energy measurements mode.

Figure 2. Example of computer ray tracing for the three-gate design (referred to as design no. 1.1). Particles enter instrument at top of diagram. Bias voltages (ϕ_1, ϕ_2, ϕ_3) are applied to the diagonal surfaces, with the polarity indicated by the $+, -$ signs. The stacked array of deflection plates focusses particles through the instrument. Forcing the particles to follow the curved path in the lower section allows a differential measurement of energy.

Figure 3. Data for DIFPM design no. 1.1. (a) Trajectories to be used for energy analysis. (b) Particle flux for each trajectory shown in part (a). A voltage sweep is applied to ϕ_2 and the opposite polarity applied to ϕ_3 while ϕ_1 and ϕ_4 remain constant. (c) Preliminary energy calibration curve with the indicated slope.

Figure 4. Data for DIFPM design no. 1.1. (a) Trajectories to be used for ion mass analysis. (b) Particle flux for each trajectory shown in part (a). A voltage sweep is applied to ϕ_3 while ϕ_1, ϕ_2, and ϕ_4 remain constant. The dotted data result from cross talk between channels.

Figure 5. Computer ray tracing for the "four-gate" design of the DIFPM (referred to as design no. 2.1).

Figure 6. Angular response for DIFPM design no. 2.1. A voltage sweep is applied to ϕ_1 while ϕ_2, ϕ_3, ϕ_4, and ϕ_5 remain constant at zero volts. Plasma conditions are ion mass $= N_2^+$ and beam energy = 37 eV. For angles 30° – 45°, the DIFPM output has been multiplied by two.

Figure 7. Angular calibration curves for design no. 2.1. For comparison the characteristics of the Spacelab-2/DIFP instrument are included. (*a*) Angle calibration: (plate voltage at peak response/particle energy) versus angle-of-attack. (*b*) Angular sensitivity: normalized current versus angle of attack.

Figure 8. Data for DIFPM design no. 2.1. (*a*) Trajectories to be used for energy analysis. (*b*) Particle flux for each trajectory shown in part (*a*). A voltage sweep is applied to ϕ_2 and the opposite polarity applied to ϕ_3 while ϕ_1, ϕ_4, and ϕ_5 remain constant. (*c*) Energy calibration curve with the indicated linear fit. The values for the positive and negative peaks (∗) have been averaged for this plot.

Figure 9. Comparison of instrument response for the energy analysis trajectories at different angles of attack to the probe.

Figure 10. Data for DIFPM design no. 2.1. (*a*) Trajectories to be used for ion mass analysis. (*b*) Particle flux for each trajectory shown in part (*a*). ϕ_1 is held constant while the remaining plates are all swept with the same voltage magnitude. The polarity is indicated in part (*a*). (*c*) Peak voltage versus energy with the indicated linear fit. The values for the positive and negative peaks (∗) have been averaged for this plot.

Figure 11. Comparison of instrument response at an angle of attack = −20° for both the

energy analysis and mass analysis trajectories.

Figure 12. Instrument response for DIFPM design no. 2.1 during time-of-flight measurement. The particle trajectory shown by the dashed line in Fig. 10*a* is chosen by selecting the voltage for the first peak (*) observed in Fig. 10*b*. The modulation frequency of the voltage amplitude is then swept. (*a*) Signature for different masses at a constant beam energy. The arrows indicate the main peak. Other peaks are ghost peaks caused by different trajectories than that described above. (*b*) Signature for different beam energies of the same mass. The arrows indicate the main peak.

Figure 13. Mass (time-of-flight) calibration curve for DIFPM design no. 2.1: frequency value of main peak versus particle velocity. The data follow a linear behavior with the indicated parameters. By using the energy calibration curve shown in Fig. 8*c* together with the time-of-flight curve shown here, one can determine the composition of an unknown plasma stream.

Figure 14. Instrument response for DIFPM design no. 2.1 during time-of-flight measurement for different angles-of-attack for constant ion mass and beam energy. The baseline for each curve has been shifted.

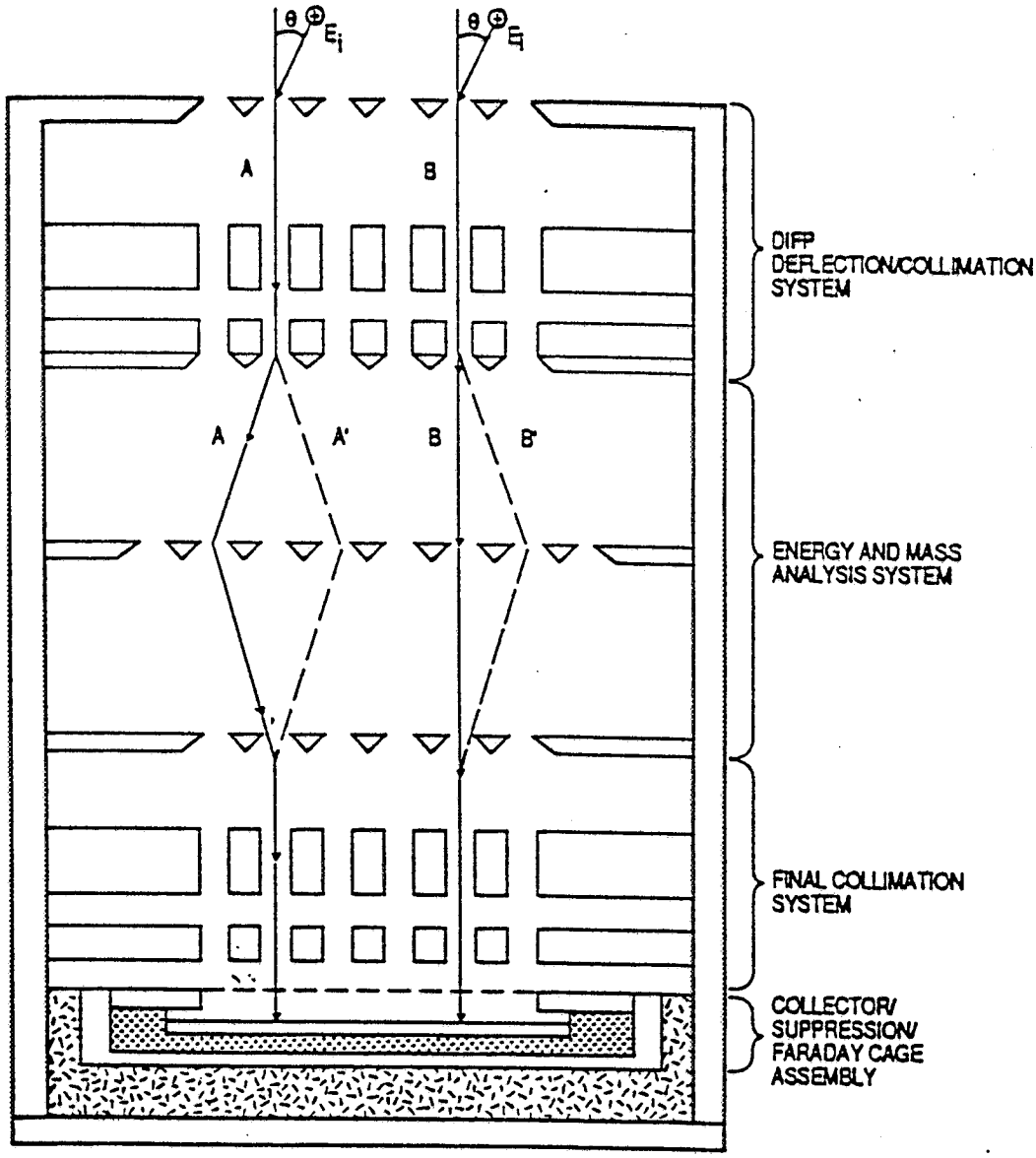
θ
E_i
θ
E_i
A
B
A
A'
B
B'
DIFP
DEFLECTION/COLLIMATION
SYSTEM
ENERGY AND MASS
ANALYSIS SYSTEM
FINAL COLLIMATION
SYSTEM
COLLECTOR/
SUPPRESSION/
FARADAY CAGE
ASSEMBLY

Fig. 1

DIFPM

PARTICLE RAY TRACES

ENERGY = 3.8 eV

ANGLE (θ) = 20°

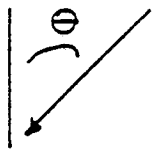

ϕ_1 = 7 v.

ϕ_2 = 10 v.

ϕ_3 = 20 v.

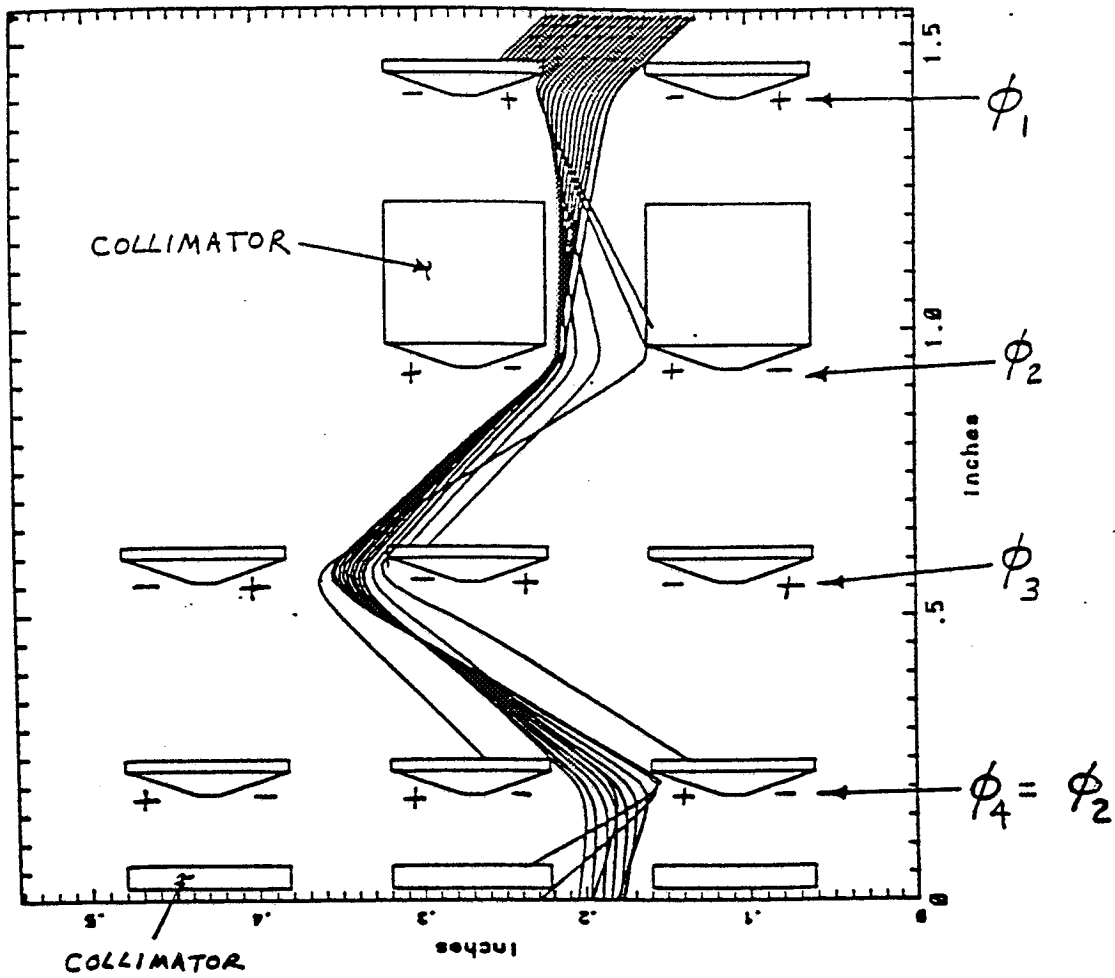

Fig. 2

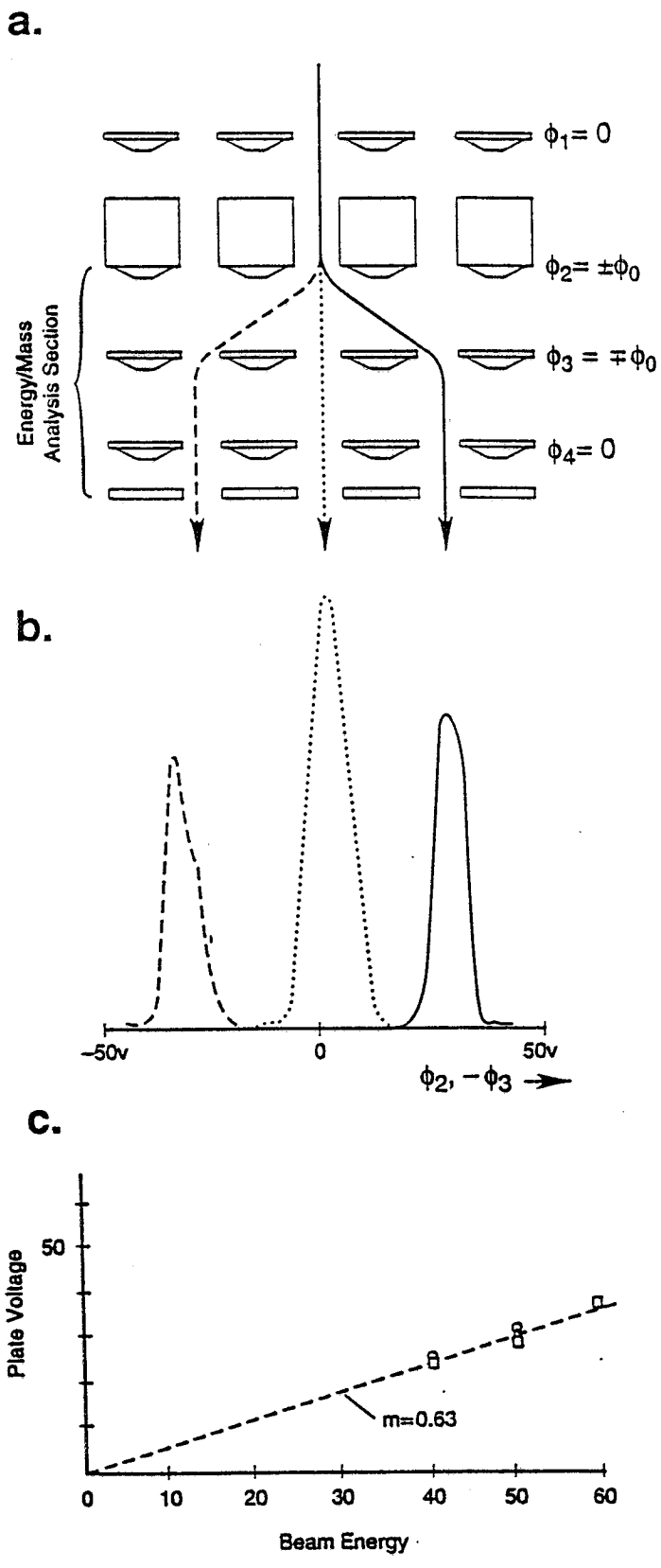
a.
$\phi_1 = 0$
$\phi_2 = \pm\phi_0$
$\phi_3 = \mp\phi_0$
$\phi_4 = 0$
Energy/Mass
Analysis Section
b.
-50v
0
50v
$\phi_2, -\phi_3$
c.
Plate Voltage
50
m=0.63
0
10
20
30
40
50
60
Beam Energy

Fig. 3

a.

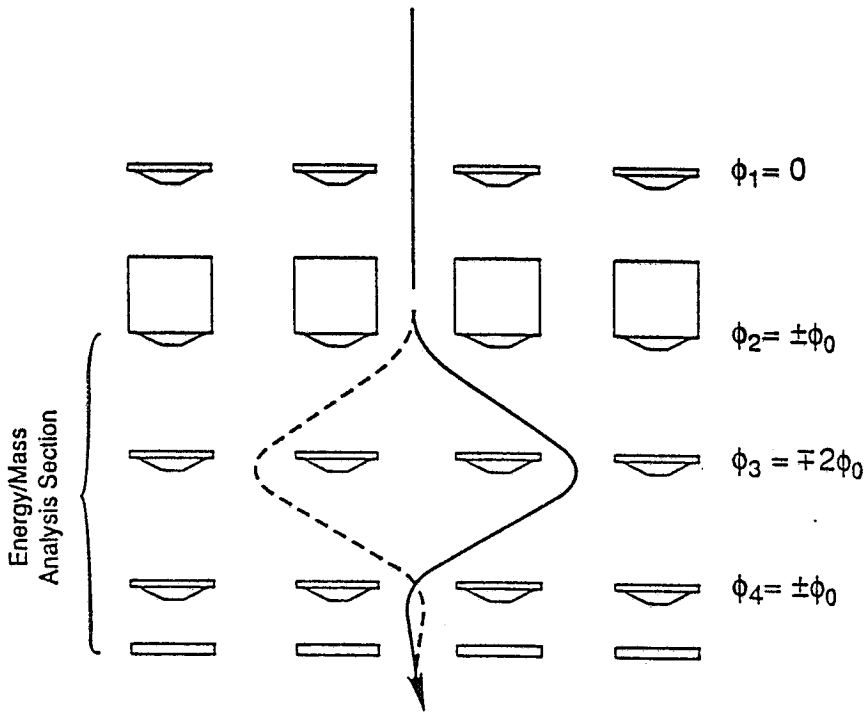
$\phi_1 = 0$
$\phi_2 = \pm\phi_0$
$\phi_3 = \mp 2\phi_0$
$\phi_4 = \pm\phi_0$
Energy/Mass
Analysis Section

b.

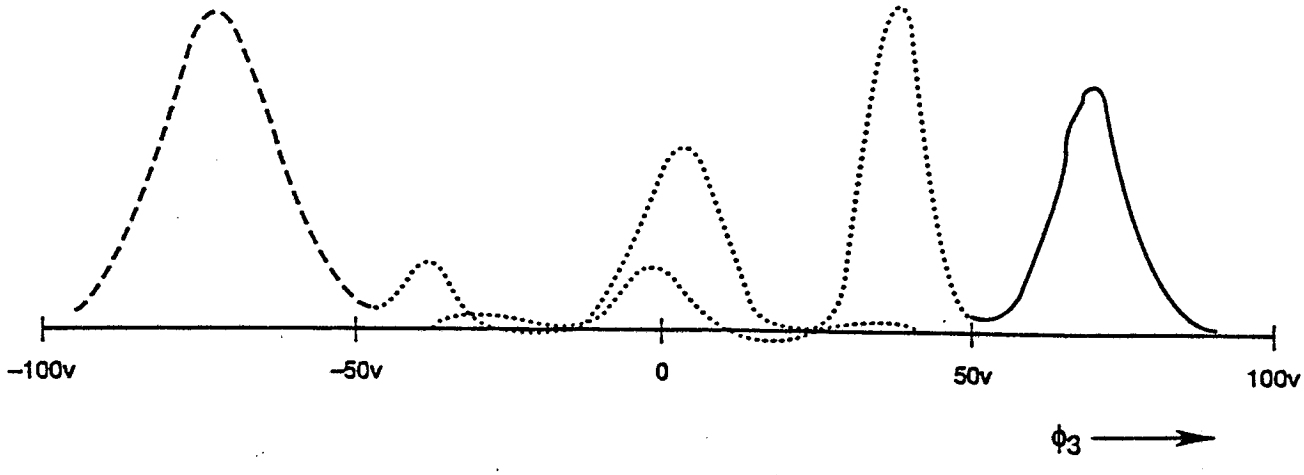
-100v
-50v
0
50v
100v
ϕ_3

Fig. 4

DIFPM
PARTICLE RAY TRACES

ENERGY = 4.8 eV
ANGLE = 0°

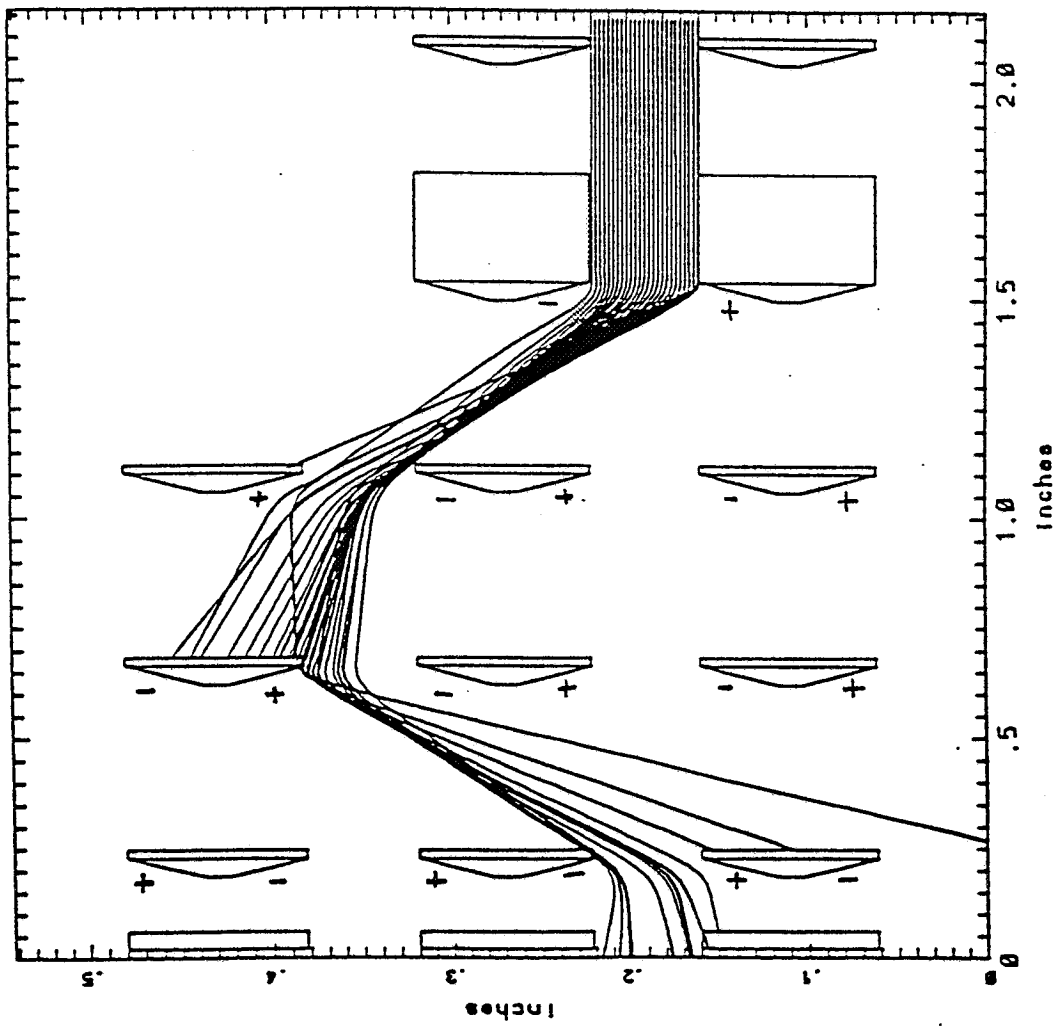

$\phi_1 = 0$

$\phi_2 = 10$ v.

$\phi_3 = 10$ v

$\phi_4 = 10$ v

$\phi_5 = 10$ v

Fig. 5

MASS = N_2^+

ENERGY = 37 eV

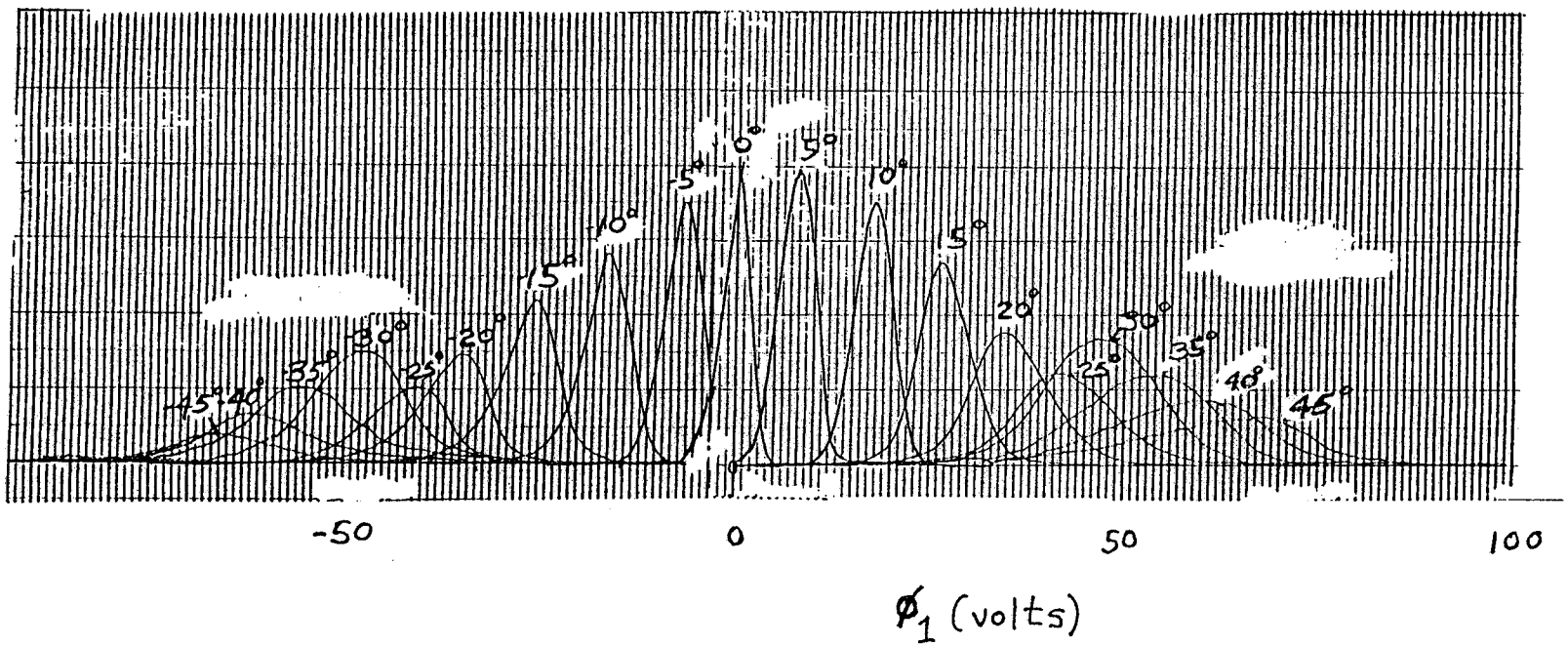

Fig. 6

a.

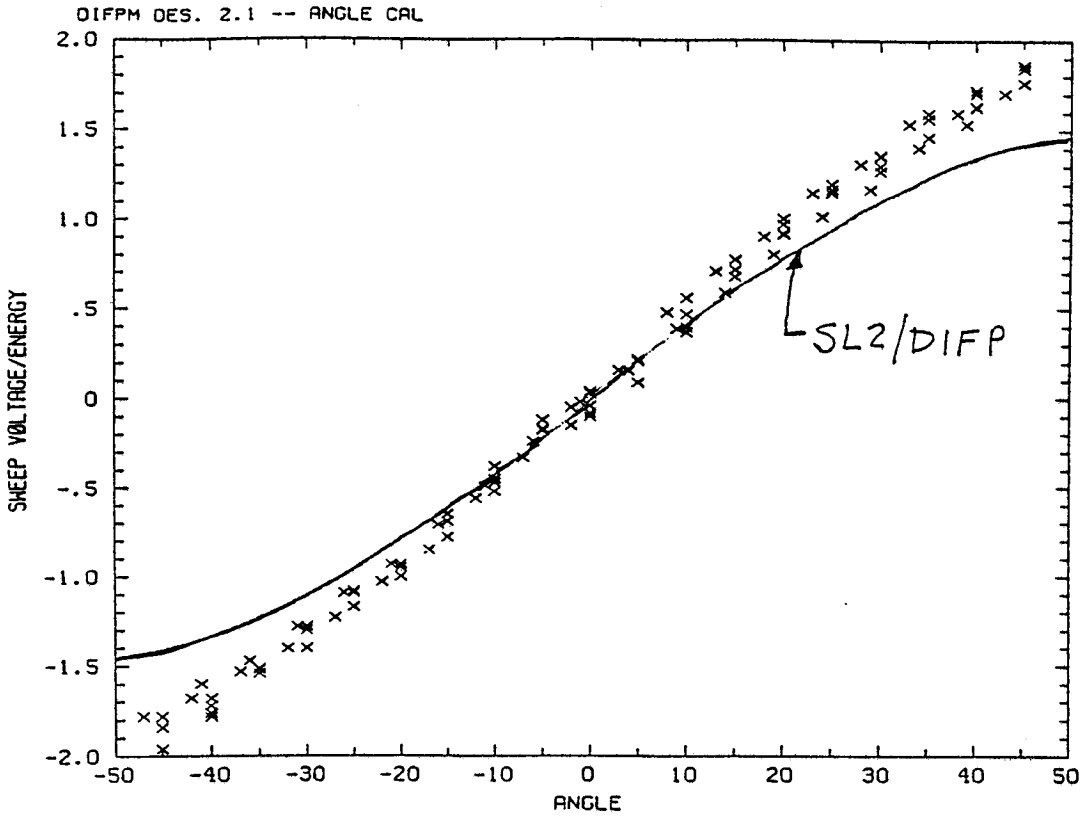
DIFPM DES. 2.1 -- ANGLE CAL
SWEEP VOLTAGE/ENERGY
ANGLE
SL2/DIFP

b.

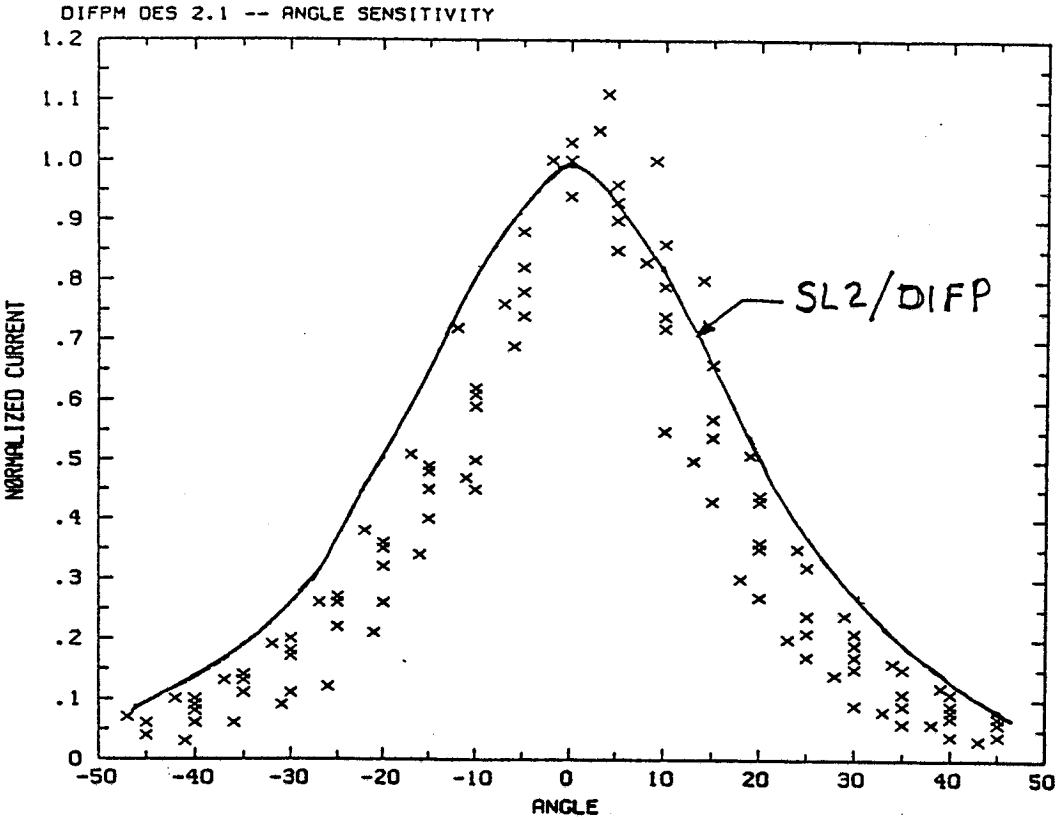
DIFPM DES 2.1 -- ANGLE SENSITIVITY
NORMALIZED CURRENT
ANGLE
SL2/DIFP

Fig. 7

a.

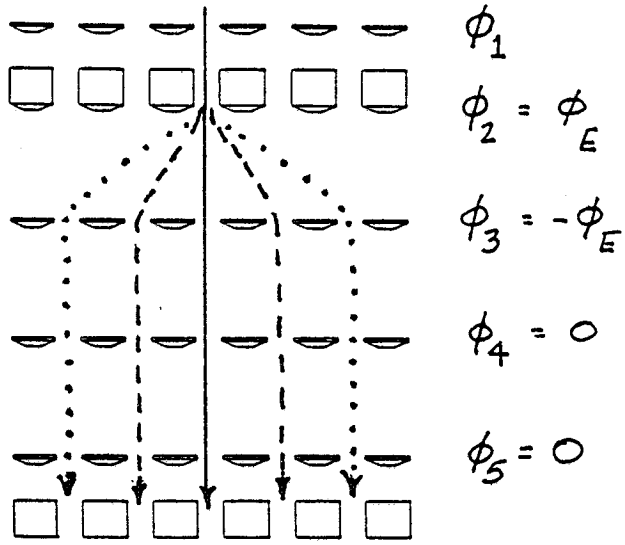
ϕ_1
$\phi_2 = \phi_E$
$\phi_3 = -\phi_E$
$\phi_4 = 0$
$\phi_5 = 0$

b.

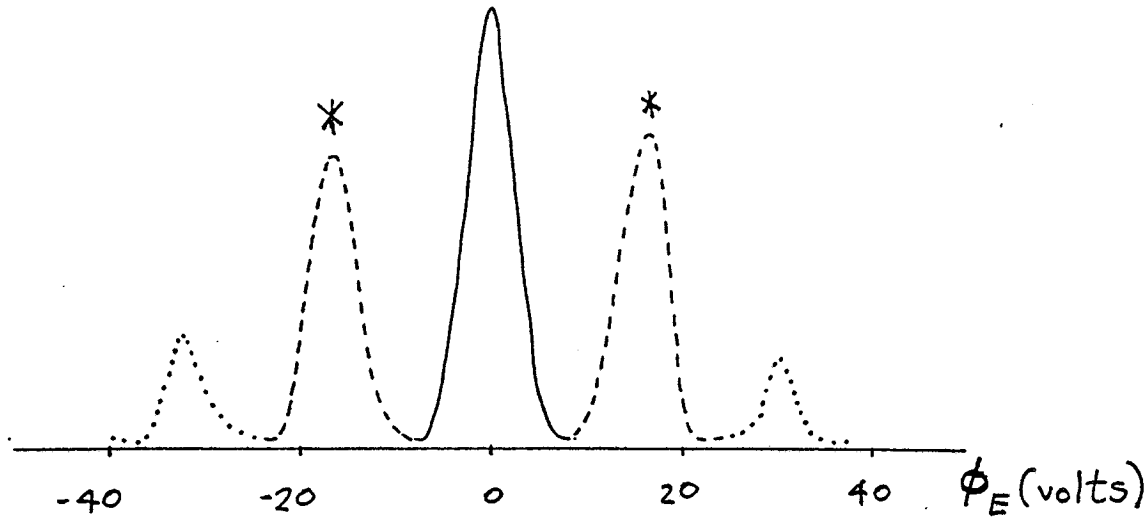
-40
-20
0
20
40
ϕ_E (volts)

C.

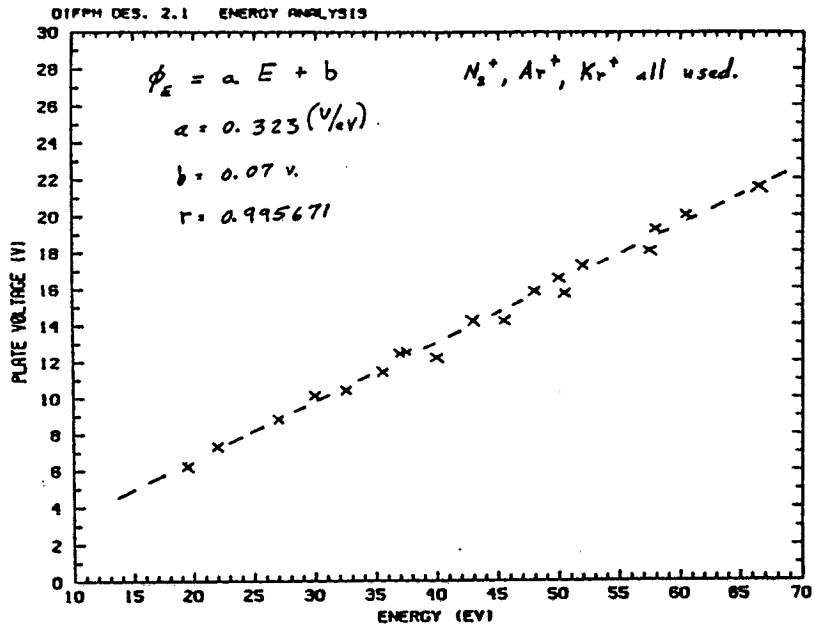
DIFFH DES. 2.1 ENERGY ANALYSIS
$\phi_E = a\ E + b$
N_2^+, Ar^+, Kr^+ all used.
a = 0.323 (V/eV)
b = 0.07 v.
r = 0.995671
PLATE VOLTAGE (V)
ENERGY (EV)

Fig. 8

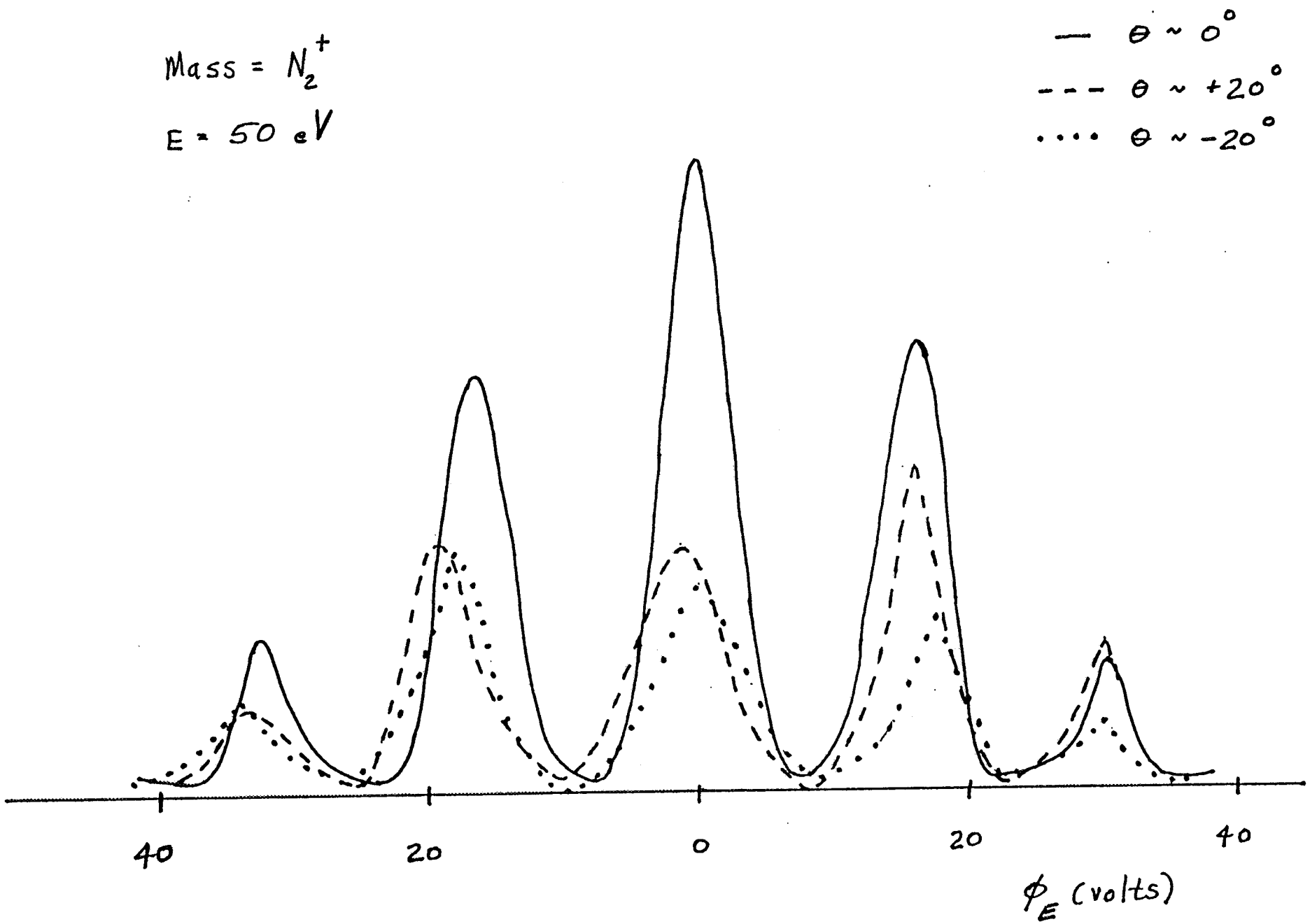

Fig. 9

a.

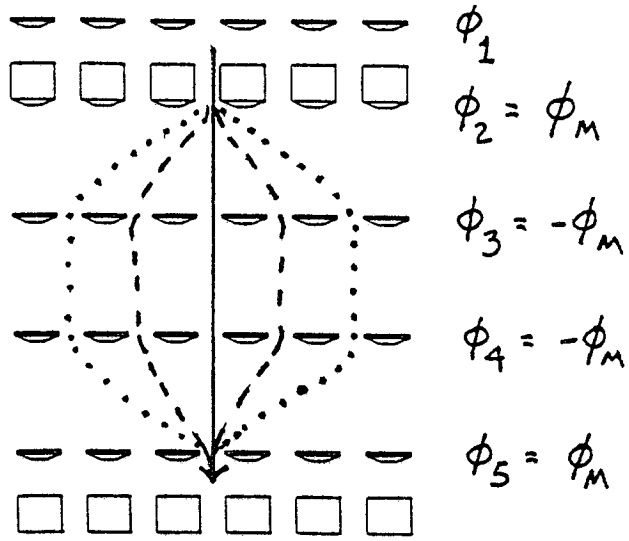
ϕ_1
$\phi_2 = \phi_M$
$\phi_3 = -\phi_M$
$\phi_4 = -\phi_M$
$\phi_5 = \phi_M$

b.

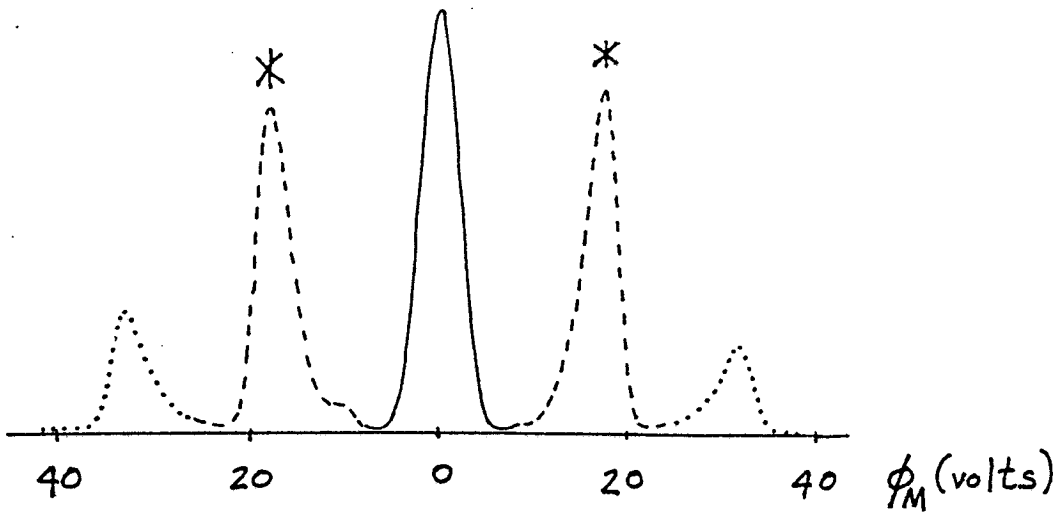
40
20
0
20
40
ϕ_M (volts)

c.

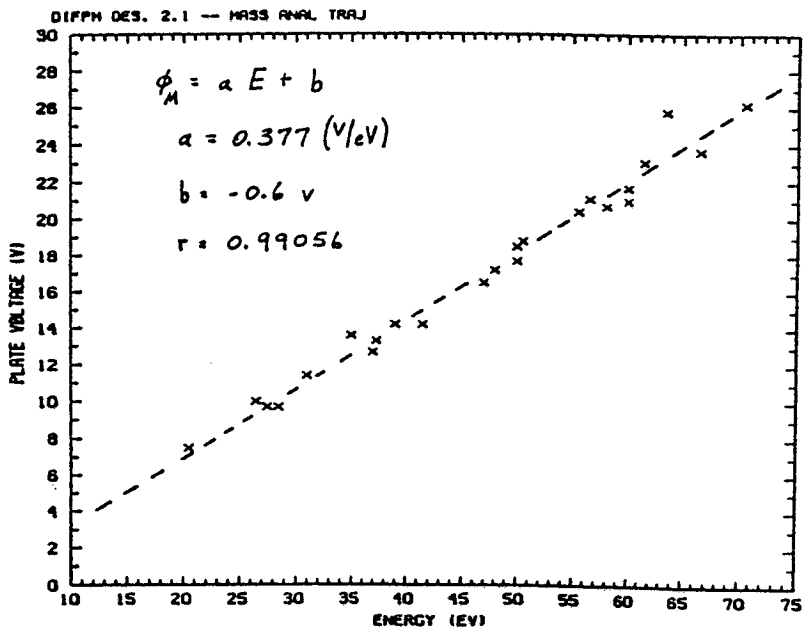
DIFFM DES. 2.1 — MASS ANAL TRAJ
$\phi_M = a E + b$
a = 0.377 (V/eV)
b = -0.6 v
r = 0.99056
PLATE VOLTAGE (V)
ENERGY (EV)

Fig. 10

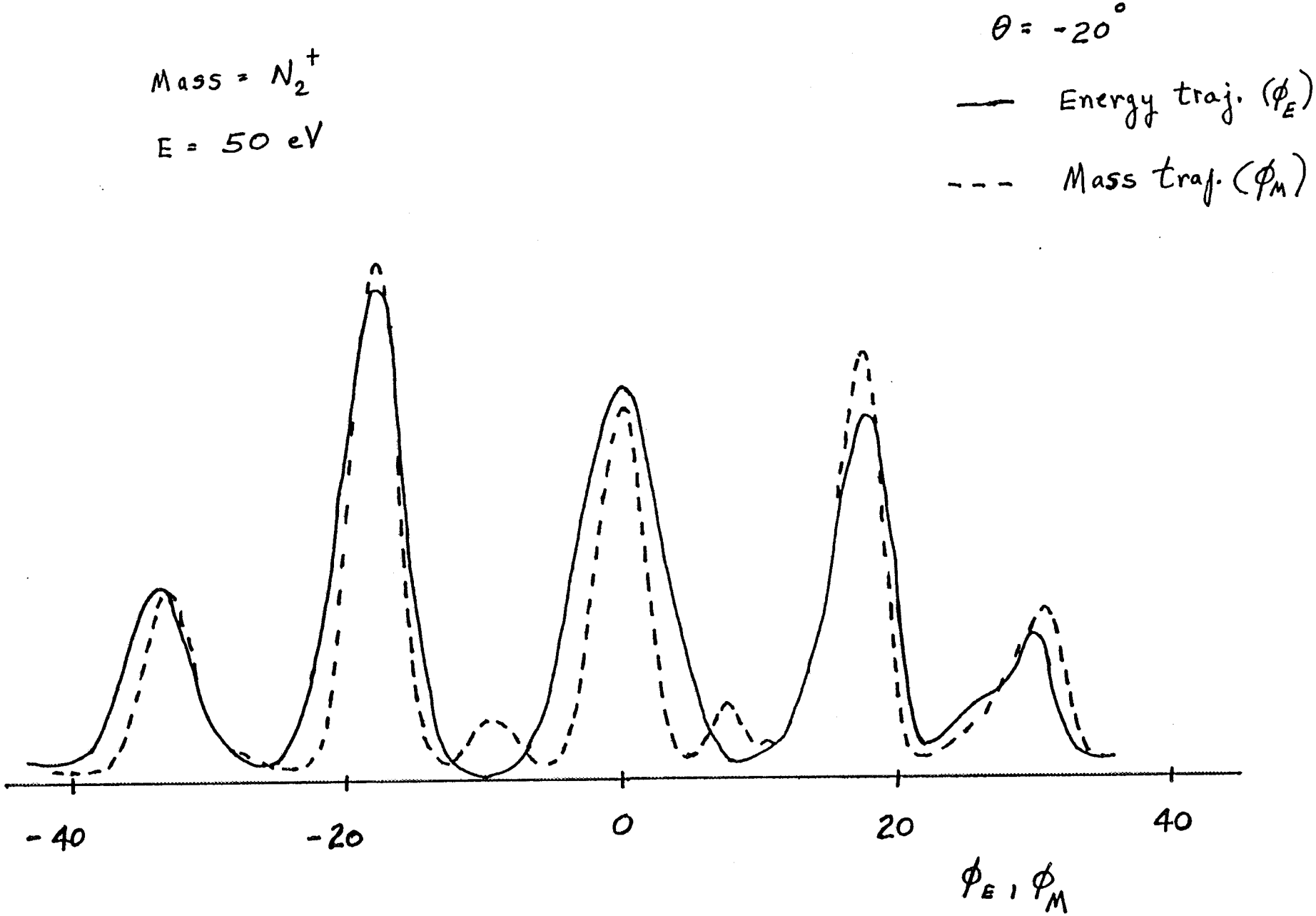
Mass = N_2^+
E = 50 eV
$\theta = -20^\circ$
Energy traj. (ϕ_E)
Mass traj. (ϕ_M)
-40
-20
0
20
40
ϕ_E , ϕ_M

Fig. 11

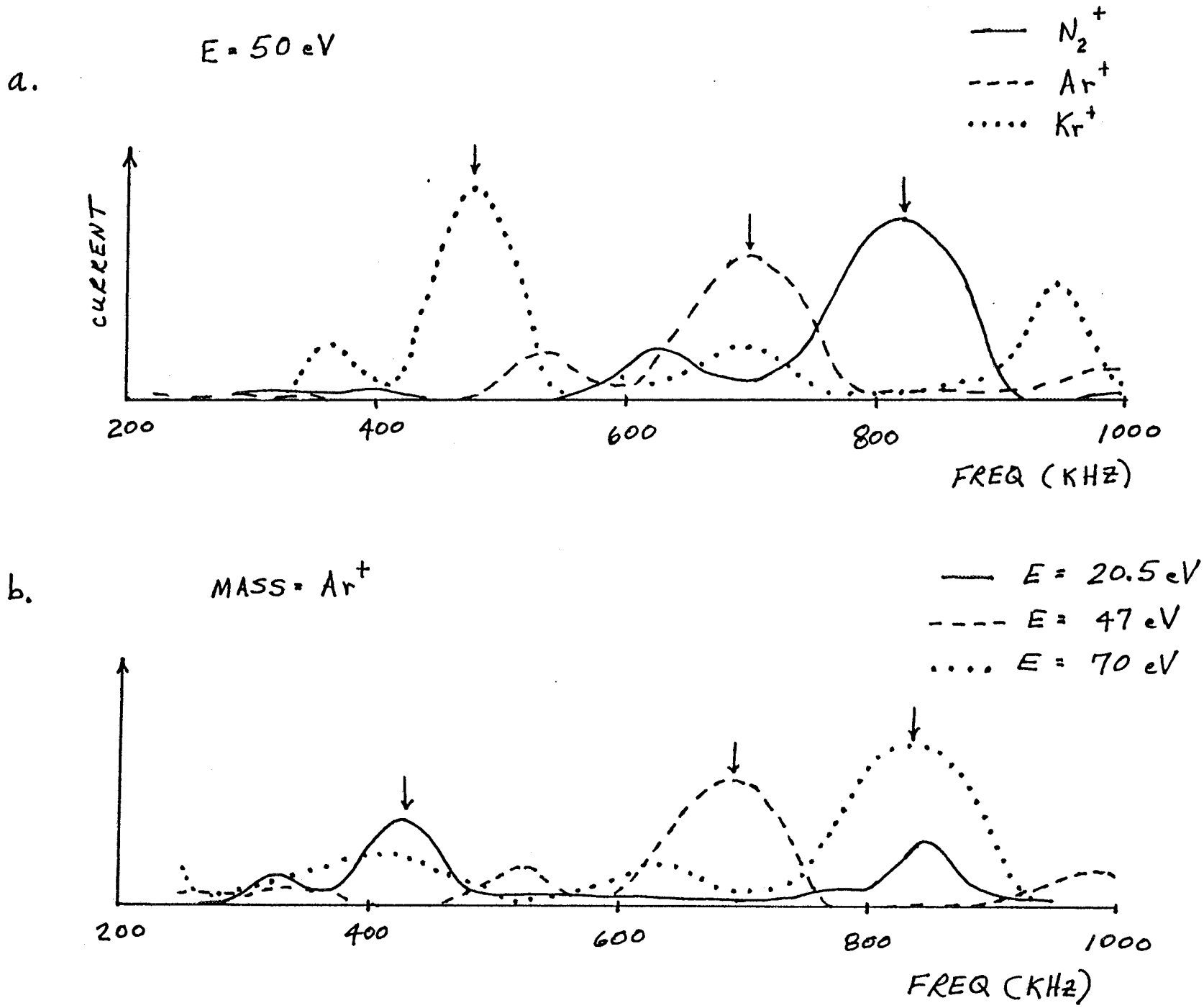
a.
E = 50 eV
N_2^+
Ar^+
Kr^+
CURRENT
200
400
600
800
1000
FREQ (KHZ)
b.
MASS = Ar^+
E = 20.5 eV
E = 47 eV
E = 70 eV
200
400
600
800
1000
FREQ (KHz)

Fig. 12

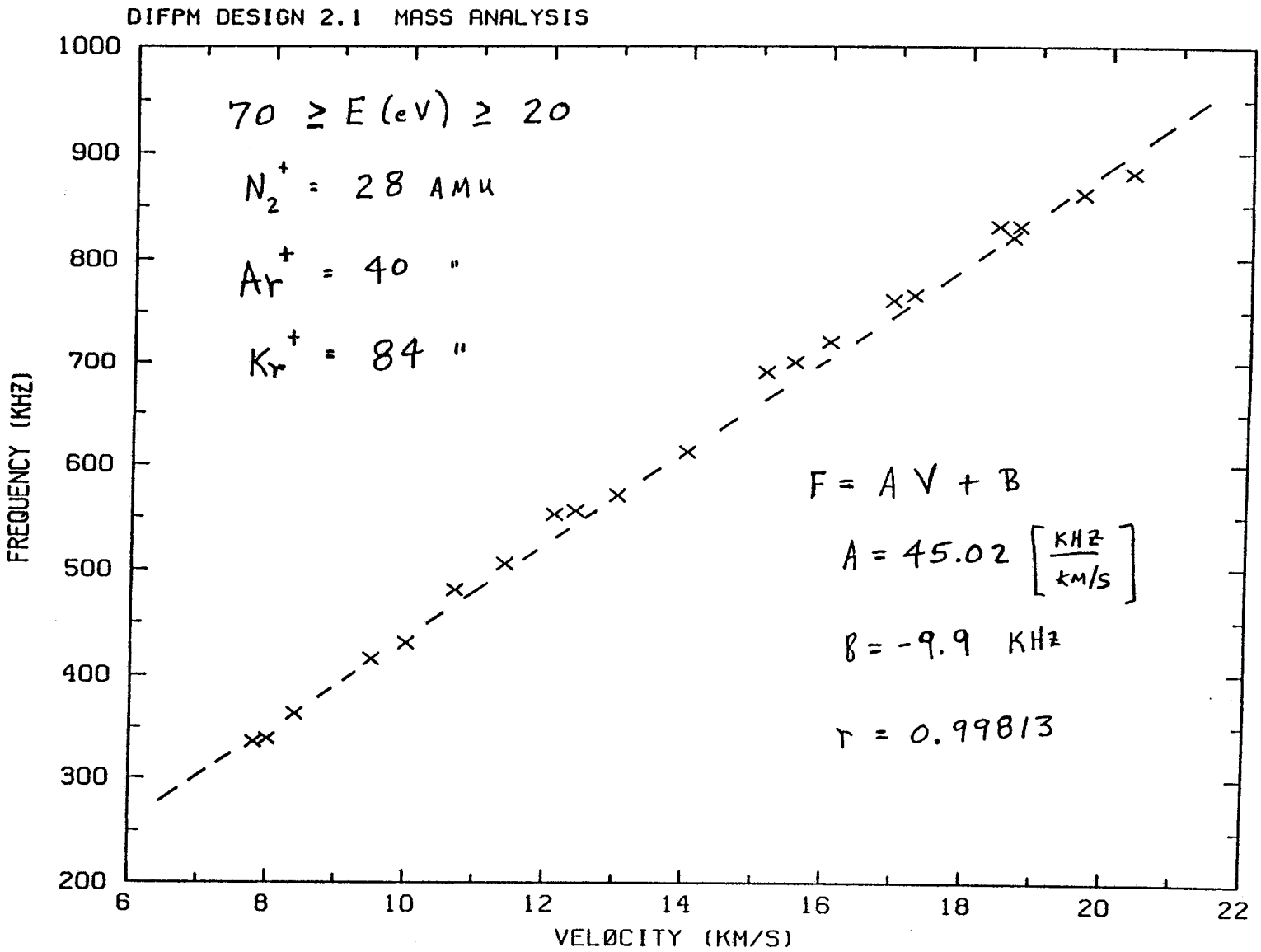
DIFPM DESIGN 2.1 MASS ANALYSIS
70 ≥ E (eV) ≥ 20
N2+ = 28 AMU
Ar+ = 40 "
Kr+ = 84 "
F = A V + B
A = 45.02 [KHz / km/s]
B = -9.9 KHz
r = 0.99813
FREQUENCY (KHZ)
1000
900
800
700
600
500
400
300
200
6
8
10
12
14
16
18
20
22
VELOCITY (KM/S)

Fig. 13

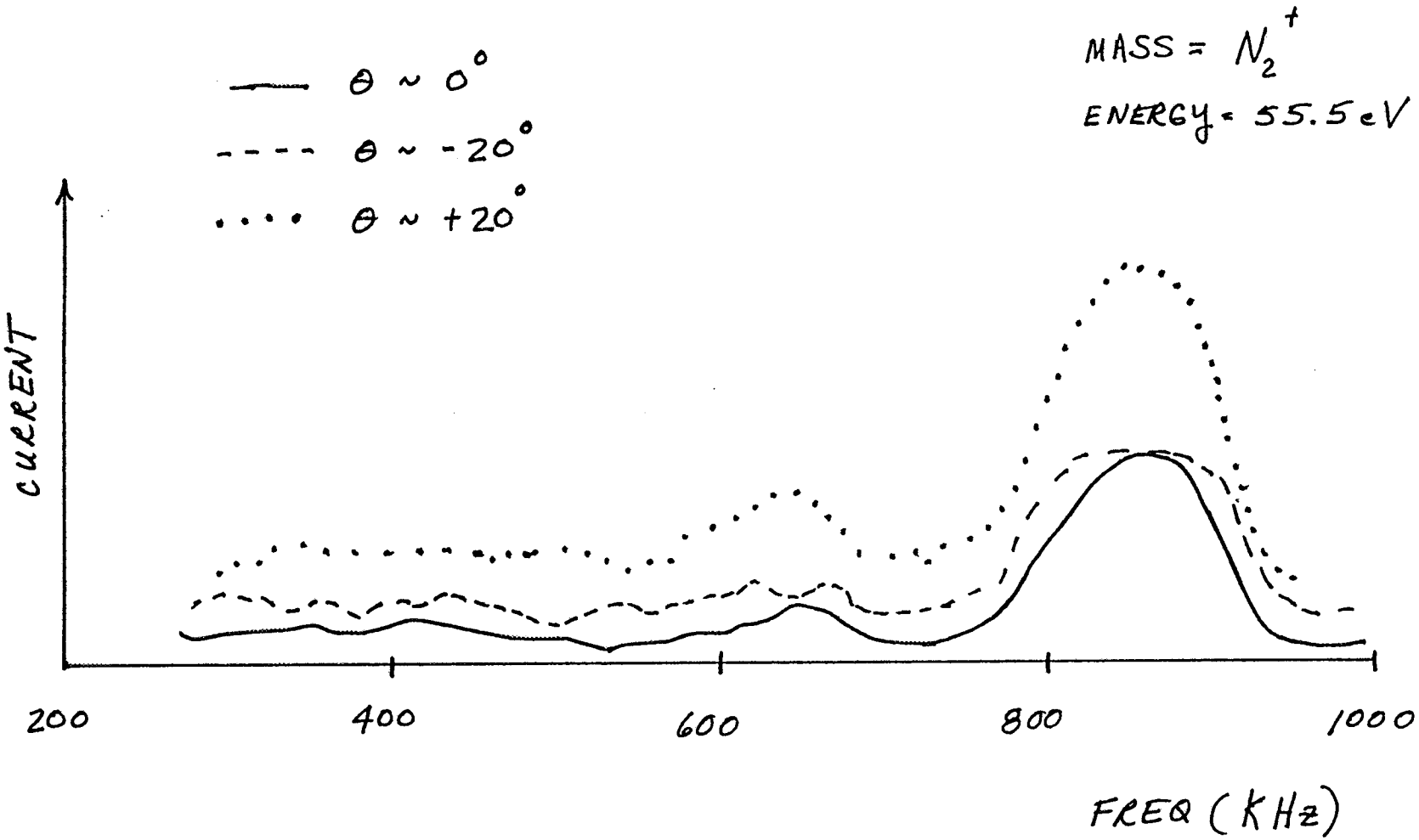
MASS = N_2^+
ENERGY = 55.5 eV
θ ~ 0°
θ ~ -20°
θ ~ +20°
CURRENT
200
400
600
800
1000
FREQ (KHz)

Fig. 14

DOC #: 30497 ABSTRACT SCREEN PAGE: 1 ** WORDS NOT FOUND *

Mass analysis addition to the Differential Ion Flu
x Probe (DIFP) study DIFP

ABQ: NC
ABA: Author (revised)

CIN: SAF
KIN: EJS
AIN:

The objective of this study is to develop a technique to measure the characteristics of space plasmas under highly disturbed conditions; e.g., non-Maxwellian plasmas with strong drifting populations and plasmas contaminated by spacecraft outgassing. The approach, conducted in conjunction with current MSFC activities, is to extend the capabilities of the Differential Ion Flux Probe (DIFP) to include a high throughput DIFP mass measurement that does not require either high voltage or contamination sensitive devices such as channeltron electron multipliers or microchannel plates. This will significantly reduce the complexity and expense of instrument fabrication, testing, and integration of flight hardware compared to classical mass analyzers. The feasibility of the enhanced DIFP has been DIFP verified by using breadboard test models in a controlled plasma environment. The ability to manipulate particles through the instrument regardless of incident angle, energy, or ionic component has been amply demonstrated. The energy AMPLY analysis mode is differential and leads

PF1=ABA LIST; PF2=RESET; PF3=SIGNON; PF4=RELEASE FROM SUBQ; PF5=SELECTION;
PF6=SUBQUEUE; PF7=STORE ABSTRACT; PF8=MAI; PF10=SEND TO 'MAIQ';
PF14=PREVIOUS PAGE; PF15=NEXT PAGE; PF19=TITLE-EXT; PF20=INDEX TERMS
4B• A =-•PC LINE 11 COL 2

DOC #: 30497 ABSTRACT SCREEN PAGE: 2 ** WORDS NOT FOUND *

Mass analysis addition to the Differential Ion Flu
x Probe (DIFP) study DIFP

ABQ: NC
ABA: Author (revised)

CIN: SAF
KIN: EJS
AIN:

directly to a time-of-flight mass measurement. With the new design, the DIFP will separate multiple ion streams and analyze each stream independently for ion flux intensity, velocity (including direction of motion), mass, and temperature (or energy distribution). In particular, such an instrument will be invaluable on follow-on electrodynamic TSS missions and, possibly, for environmental monitoring on the space station.

DIFP

PF1=ABA LIST; PF2=RESET; PF3=SIGNON; PF4=RELEASE FROM SUBQ; PF5=SELECTION;
PF6=SUBQUEUE; PF7=STORE ABSTRACT; PF8=MAI; PF10=SEND TO 'MAIQ';
PF14=PREVIOUS PAGE; PF15=NEXT PAGE; PF19=TITLE-EXT; PF20=INDEX TERMS
4B• A =-•PC LINE 11 COL 2

DOC NUMBER: 30497 INDEXING: SUBJECT/TERMS SCREEN CIN: SAF
TITLE: Mass analysis addition to the Differential Ion Flu KIN: EJS
x Probe (DIFP) study AIN:

	MAJOR TERMS:	SWITCH
1:	FLUX (RATE)	_
2:	SPACE PLASMAS	_
3:	CONTAMINATION	_
4:	OUTGASSING	_
5:	HIGH VOLTAGES	_
6:	PHOTOMULTIPLIER TUBES	_
7:	TIME OF FLIGHT SPECTROMETERS	_
8:	MASS DISTRIBUTION	_
9:	design analysis	_
10:		_
11:		_
12:		_
13:		_
14:		_
15:		_

	MINOR TERMS:	
1:	TEMPERATURE DISTRIBUTION	_
2:	ENVIRONMENTAL MONITORING	_
3:	SPACE STATIONS	_
4:	SENSITIVITY	_
5:	MICROCHANNEL PLATES	_
6:	BREADBOARD MODELS	_
7:	CHANNEL MULTIPLIERS	_
8:	MAGNETOSPHERES	_
9:	RAY TRACING	_
10:		_
11:		_
12:		_
13:		_
14:		_
15:		_

PROPOSED TERMS:

PF2=RESET; PF3=SIGNON; PF4=RELEASE; PF5=SELECTION; PF6=SUBQ
PF10=ALPHA; PF11=HIERARCHY; PF12=STORE; PF13=CENTRAL SCREEN; PF20=TITLE/WNF
4B• A =-•PC LINE 14 COL 26